Quantitative Two-Dimensional Ultrashort Echo Time Magnetization Transfer (2D UTE-MT) Imaging of Cortical Bone

Ya-Jun Ma[1], **Anthony Tadros**[1], **Jiang Du**[1], and **Eric Y Chang**[2,1]

[1]Department of Radiology, University of California, San Diego, CA

[2]Radiology Service, VA San Diego Healthcare System, San Diego, CA

Abstract

Purpose—To investigate quantitative 2D ultrashort echo time magnetization transfer (UTE-MT) imaging in ex-vivo bovine cortical bone and in-vivo human tibial cortical bone.

Methods—Data were acquired from 5 fresh bovine cortical bone samples and 5 healthy volunteer tibial cortical bones using a 2D UTE-MT sequence on a clinical 3T scanner. The 2D UTE-MT sequence employed four or five MT powers with five frequency offsets. Results were analyzed with a two-pool quantitative MT model, providing measurements of macromolecular fraction (f), macromolecular proton transverse relaxation times (T_{2m}), proton exchange rates from water/macromolecular to the macromolecular/water pool (RM_{0m}/RM_{0w}) and spin-lattice relaxation rate of water pool (R_{1w}). Besides, a sequential air-drying study for a small bovine cortical bone chip was used to investigate whether above MT modeling parameters were sensitive to the water loss.

Results—Mean fresh bovine cortical bone values for f, T_{2m}, R_{1w}, RM_{0m}, and RM_{0w} were $59.9 \pm 7.3\%$, 14.6 ± 0.3 μs, 9.9 ± 2.4 s^{-1}, 17.9 ± 3.6 s^{-1} and 11.8 ± 2.0 s^{-1}, respectively. Mean in vivo human cortical bone values for f, T_{2m}, R_{1w}, RM_{0m} and RM_{0w} were $54.5 \pm 4.9\%$, 15.4 ± 0.6 μs, 8.9 ± 1.1 s^{-1}, 11.5 ± 3.5 s^{-1} and 9.5 ± 1.9 s^{-1}, respectively. Besides, the sequential air-drying study shows that f, RM_{0m} and R_{1w} were increased with longer drying time.

Conclusion—UTE-MT two-pool modeling provides novel and useful quantitative information for cortical bone.

Keywords

ultrashort echo time; magnetization transfer; two-pool modeling; cortical bone

Introduction

Osteoporotic fractures, such as of the hip and vertebra, have a very high morbidity and mortality (1). With a lifetime risk of approximately 40–50% for women and 13–22% for men, osteoporotic fractures are generally defined as occurring at sites of low bone mineral density (BMD) (2). Although BMD is considered the standard measure for the diagnosis of

Corresponding Author: Eric Y Chang, M.D., ericchangmd@gmail.com, VA San Diego Healthcare System, San Diego, CA 92161, Phone: 858-642-1221.
The first two authors have equal contributions

osteoporosis and assessment of fracture risk, several studies have demonstrated that BMD cannot be used as the sole predictor of bone strength. In particular, changes in BMD have been shown to account for < 50% of variation in whole bone strength (3), with the majority of fragility fractures occurring in patients with a T-score > –2.5 (4, 5). Identification of more sensitive determinants of bone strength using magnetic resonance imaging (MRI) has consequently been an active area of interest.

Due to the short T_2 components of bone matrix, clinical MRI systems are generally limited to the imaging of the marrow space. While high resolution MRI has been shown to detect age and disease-induced changes in trabecular morphology (6), the use of ultrashort echo time (UTE) pulse sequences has allowed for the quantitative evaluation of cortical bone (7–10). Water content and T_2^* measurements have been shown to correlate with cortical bone porosity and failure properties (8, 10). Despite that, protons with extremely fast transverse relaxation, such as tightly bound water and collagen protons, remain undetectable even when UTE is employed. Magnetization transfer (MT) imaging has therefore been investigated as a potential method to indirectly assess these "invisible" proton pools.

The MT technique generates unique contrast and quantitative information in MRI by exploiting coupling processes between macromolecular and mobile protons. MT imaging uses an off-resonance radiofrequency (RF) pulse to preferentially saturate macromolecular protons. Since macromolecular protons can influence the spin state of mobile protons, this off-resonance saturation can be subsequently transferred to mobile protons and thereby be measured by MRI. The extent of magnetization transfer between these two pools of protons depends on their rate of exchange (11). In combination with UTE (UTE-MT), MT has been studied as a quantitative measure of short T_2 tissues (12, 13). More recently, magnetization transfer ratios (MTR) using the UTE-MT technique have been shown to be sensitive to cortical bone porosity, as determined by μCT, and biomechanical function (14).

To improve the sensitivity and reproducibility of MT metrics in cortical bone, we sought to explore a more quantitative modeling of MT phenomena in combination with UTE. We aimed to optimize acquisition protocols and better understand MT behavior in ex vivo bovine and in vivo healthy human tibial cortical bone. Our purpose was to establish methods enabling UTE-MT two-pool modeling measurements that might potentiate new surrogate markers for cortical bone strength.

Methods

Two-Pool MT Modeling

Two-pool MT modeling was performed to measure macromolecular fraction (f), water proton transverse relaxation time (T_{2w}), macromolecular proton transverse relaxation time (T_{2m}), proton exchange from water to macromolecular pool (RM_{0m}), and proton exchange from the macromolecular to water pools (RM_{0w}). Two-pool UTE-MT modeling was largely based on the previously described Ramani model (15), in which the MT pulse was treated as a rectangular continuous wave (CW) signal with the same mean saturating power as the experimentally used shaped pulse, or the so-called continuous wave power equivalent (CWPE) approximation. The angular frequency of precession w_{CWPE} induced by the off-

resonance MT pulse was used to measure the amplitude of the B_1 field. The UTE-MT signal was modeled by the following equation (15):

$$S = g M_{0w} \frac{R_{1m} \left[\frac{RM_{0w}f}{R_{1w}(1-f)} \right] + R_{RFm} + R_{1m} + RM_{0w}}{\left[\frac{RM_{0w}f}{R_{1w}(1-f)} \right](R_{1m} + R_{RFm}) + \left(1 + \left[\frac{w_{\mathrm{CWPE}}}{2\pi\Delta f}\right]^2 \left[\frac{1}{R_{1w}T_{2w}}\right]\right)(R_{RFm} + R_{1m} + RM_{0w})} \quad [1]$$

where M_{om} and M_{ow} are the fully relaxed magnetizations of macromolecular and water pools, respectively. f is defined as $\frac{M_{0m}}{M_{0m}+M_{0w}}$. R_{1m} and R_{1w} are the corresponding longitudinal rate constants. g is an amplitude scaling factor. R is the first-order magnetization exchange rate constant between the two pools. R_{RFm} is the loss rate of longitudinal magnetization of the macromolecular pool due to the RF saturation of the MT pulse. Here we employ a Gaussian lineshape for the macromolecular proton pool in cortical bone due to its extremely short T_2 value (16). Additional details regarding the UTE-MT two-pool modeling used in this study have been previously reported (17).

Pulse Sequence

The 2D UTE-MT sequence employs an MT preparation pulse followed by a basic 2D UTE data acquisition. The basic 2D UTE sequence uses a hard pulse or a short half pulse excitation followed by 2D radial ramp sampling. Fast transmit/receive switching allows for a minimal nominal TE of around 10 μs (14). The MT preparation pulse is a Fermi pulse with a duration of 8 ms, a spectral bandwidth of 0.8 kHz, a maximal B_1 of 24μT and a maximal saturation flip angle of 1740°. The Fermi pulse was employed because it provided an improved spectral profile compared with a rectangular pulse and higher efficiency compared with conventional Gaussian or sinc pulses, facilitating MT modeling of cortical bone, which has an extremely short apparent transverse relaxation time or T_2*. 2D UTE-MT data were acquired with a series of MT pulse frequency offsets (f) and powers (ω_1) for two-pool MT modeling.

Ex Vivo UTE-MT Imaging

In total, five mature bovine femoral and tibial midshafts from freshly slaughtered animals were obtained from a local slaughterhouse and cleaned of external muscle and soft tissue. A bovine cross-section with approximate thickness of 4 cm was cut from each specimen using a low-speed diamond saw (Isomet 1000, Buehler) with constant water irrigation, and stored in phosphate buffered saline (PBS) solution for 24 hours prior to use. A wrist coil (BC-10, Medspira, Minneapolis, MN) was used for both signal excitation and reception. The 2D non-selective UTE-MT imaging protocol included: TR=100 ms, TE=10 μs, FOV=8×8 cm^2, hard excitation pulse (32 μs) with a flip angle =10°, acquisition matrix=128×128, five MT powers (300°, 600°, 900°, 1200° and 1500°) and five MT frequency offsets (2, 5, 10, 20 and 50 kHz), with a total of 25 different MT datasets. The total scan time was about 17.5 min. T_1 values were measured with the same UTE sequence except without MT preparation using a rectangular excitation pulse (duration = 80 μs) with a flip angle=25° and multiple TRs (i.e. 24, 50, 100, 200, 400, 600, 800 ms). Then T_1 was calculated by fitting the following equation (18, 19):

$$S = S_0 e^{-\frac{TE}{T_2^*}} \frac{1 - e^{-\frac{TR}{T_1}}}{1 - \cos(\theta) e^{-\frac{TR}{T_1}}} \quad [2]$$

Where S_0 is the signal intensity in the equilibrium state and TE is a constant. Therefore, the first two elements in the above equation can be combined into a constant when fitting. Total scan time was about 15.2 min.

A sequential air-drying study was also performed to investigate whether UTE-MT modeling parameters are sensitive to the water content loss in cortical bone. A bovine cortical bone chip was cut with approximate dimensions of $18 \times 12 \times 5$ mm^3. The bone chip was immersed in PBS for 30 mins before the first experiment. The second and third experiments were conducted after one and three hours of air-drying in a 22°C condition, respectively. A 30 ml birdcage coil was used for both RF transmission and signal reception. The sequence parameters were identical to the above bovine cortical bone sample study.

Reproducibility was investigated for the two-pool UTE-MT modeling of cortical bone with three measurements. The MRI system was reset before each measurement and the same slice location was used for all the measurements. Mean and standard deviation values of the three independent measurements were calculated.

In Vivo UTE-MT Imaging

The 2D UTE-MT sequence was also applied to the tibial midshaft of five healthy volunteers (all males, 28–43 years old, mean/standard deviation=32.6±6.4 y) for two-pool modeling. Written informed consent approved by our Institutional Review Board was obtained prior to their participation in this study. An 8-channel knee coil was used for signal excitation and reception. The protocol was similar to that for the bovine specimens, except for the use of a soft half pulse excitation with variable rate selective excitation (VERSE) (pulse duration=472μs, pulse bandwidth=2.7 kHz), FOV=10×10cm^2, slice thickness of 7mm, acquisition matrix=192×192, and four MT powers (600°, 900°, 1200° and 1500°) for a total scan time of 14 min. T_1 value was measured with a similar 2D selective UTE sequence (flip angle=25°) and TRs=10, 40, 70, 100, and 150 ms for a scan time of 2.6 min.

Data Analysis

The analysis algorithm was written in MATLAB 2012a (MathWorks Inc., Natick, MA, USA) and was executed offline on the DICOM images obtained by the 2D UTE-MT protocols described above. Two-pool UTE-MT modeling was performed on the bovine femoral midshaft and human tibial midshaft cortical bones, and was performed pixelwise (i.e. quantitative mapping) as well as by using the mean values of regions of interest (ROIs) placed in each image separately. Mean and standard deviation of macromolecular proton fractions, relaxation times, exchange rates and water longitudinal relaxation rates were calculated and summarized.

Results

Figure 1 shows 2D UTE-MT images from an ex vivo bovine cortical bone sample with different MT flip angles and off-resonance frequencies. Increased cortical bone signal intensity is observed at low MT flip angles and high off-resonance frequencies. The excellent fitting curves demonstrate the validity of using the 2D UTE-MT sequence to model MT effect in cortical bone which has extremely short T2 and shows as signal void when imaged with conventional clinical sequences. Color maps of select MT modeling parameters from another bovine cortical bone specimen are presented in Figure 2. The parameter distributions of MT modeling can be seen in the analyzed region.

For the reproducibility study, mean and stand deviation values of three independent measurements for f, T_{2m}, R_{1w}, RM_{0m}, and RM_{0w} were $56.1 \pm 1.0\%$, 14.2 ± 0.02 s^{-1}, 16.9 ± 0.8 s^{-1}, 13.2 ± 0.1 s^{-1} and 8.9 ± 0.4 s^{-1}, respectively, demonstrating excellent reproducibility of the 2D UTE-MT modeling technique.

UTE-MT images from in vivo human cortical bone are shown in Figure 3. Representative images at MT flips angles of 600° and 1500° show increased cortical bone signal intensity with lower MT power and higher off-resonance frequencies. Again, excellent curve fitting was achieved for all 2D UTE-MT data acquired with different MT flip angles and off-resonance frequencies, suggesting the feasibility for fast MT modeling of cortical bone in vivo.

Quantitative MT modeling measurements of ex vivo and in vivo cortical bone are presented in Tables 1 and 2, respectively. Mean bovine cortical bone values for f, T_{2m}, R_{1w}, RM_{0m}, RM_{0w}, and residual of fitting were $59.9 \pm 7.3\%$, 14.6 ± 0.3 μs, 9.9 ± 2.4 s^{-1}, 17.9 ± 3.6 s^{-1}, 11.8 ± 2.0 s^{-1}, and $1.8 \pm 0.1\%$, respectively. Mean human cortical bone values for f, T_{2m}, R_{1w}, RM_{0m}, RM_{0w}, and residual of fitting were $54.5 \pm 4.9\%$, 15.4 ± 0.6 μs, 8.9 ± 1.1 s^{-1}, 11.5 ± 3.5 s^{-1}, 9.5 ± 1.9 s^{-1}, and $2.7 \pm 0.3\%$, respectively.

Figure 4 shows the results of the sequential air-drying study. f, RM_{0m} and R_{1w} were increased with longer drying time. In addition, almost no changes were observed in T_{2m}.

Discussion

In this study, we demonstrated that a quantitative model of MT can be performed in ex vivo bovine and in vivo human cortical bone with suitable estimates of model parameters. We found the two-pool model to appropriately describe the acquired signal as a function of off-resonance RF power and frequency with good fit.

Several pools of proton signal in cortical bone have been identified, which differ considerably in their transverse relaxation times. Horch et al. postulated six biophysical origins of NMR signal in cortical bone, including collagen methylene, collagen amides/hydroxides, mineral hydroxides/water, collagen-bound water, pore space water, and lipid methylene (20). Since most MRI techniques of cortical bone are dominated by signal from collagen-bound water and to a lesser extent pore water, most prior studies have focused on these proton pools (21–23). Several studies have shown that cortical porosity, such as from

increased bone turnover or age-related bone loss, is a major determinant of bone mechanical strength (24–28). Hence, identifying potential surrogate measures of cortical porosity has been an area of considerable interest, especially using UTE techniques. For example, subsequent in vivo studies have validated the use of UTE MRI techniques for the assessment of bound and pore water (29, 30). More recently, UTE MRI has been combined with MT technique (UTE-MT) to not only assess cortical bone water, but also the extremely short T_2 macromolecular proton pool (15, 31).

Despite the potential advantages of UTE-MT over other methods of bone quantification, UTE-MT measurements are intrinsically semi-quantitative (14). Several variables can influence MTR, including main magnetic field and RF homogeneities, inherent tissue T_1 and T_2 relaxation times, and pulse sequence application. Well established in CNS applications (32, 33), models detailing the MT process have been developed that are implementation independent with few recent studies describing this technique in musculoskeletal applications, such as in Achilles tendon and muscle (17, 34). To our knowledge, however, UTE-MT using two-pool modeling has not been previously reported in cortical bone.

Quantitative UTE-MT parameters obtained were f, T_{2m}, R_{1w}, RM_{0m}, and RM_{0w}. Previous studies show that all the MT modeling parameters are independent and can be uniquely determined (15, 16). These parameters are expected to provide information on various tissue properties. Higher MT powers can saturate macromolecular protons more effectively, allowing more accurate MT modeling. However, proper consideration should be given to the MT powers that are used because higher MT power will generate higher specific absorption ratio (SAR), which can be problematic, especially for in vivo studies. Powers up to 1500° with a TR of 100 ms represents a good balance between high saturation efficiency and SAR limitation for in vivo imaging of the tibial midshaft. For MT modeling, the acquired data with a wide range of saturation including high saturation to non-saturation conditions are needed for accurate modeling since there are a total of five fitting parameters. The macromolecular components have a broad lineshape with a T_2 around a few microseconds. Thus, a wide range of off-resonance frequencies from 2 KHz to 50 KHz and MT powers from 300° to 1500° can generate a broad range of signal saturation. To achieve relatively accurate MT modeling, the lowest off-resonance frequency is chosen in order to minimize direct saturation of the water pool. Therefore, the lowest off-resonance frequency for MT modeling of short T_2 tissues such as cortical bone (minimal off-resonance frequency offset of 2KHz) is higher than that of long T_2 tissues such as white matter and optic nerve (i.e. 1KHz).

The bound or macromolecular fraction is a measure particularly unique to quantitative MT modeling. We observed mean macromolecular fractions of 59.9 ± 7.3% and 54.5 ± 4.9% in ex vivo bovine and in vivo human tibial cortical bone, respectively. The corollary of these results is in keeping with previous measures of total water content (17.4–24.8%) among in vivo human tibial cortical bone studies (10, 35, 36). Based on NMR experiments in human cortical bone, greater than 80% of signal contributions from this observed proton fraction would be expected to correspond with collagen methylene (20). Since serum and urine collagen degradation products seen with increased bone resorption may be confounded by various factors such as circadian rhythm, fracture healing and others (37), cortical bone

bound fraction might be complementary to existing methods used for treatment monitoring and fracture risk prediction. The disease specificity of such a measure however must be determined in patient studies prior to forming a conclusion on the clinical use of quantitative UTE-MT in cortical bone.

For the sequential air-drying study, f, RM_{0m} and R_{1w} are increased with longer drying time. f is increasing due to more water loss with a longer drying time. With air-drying, free water can be lost much more quickly than bound water (38). As a result, bound water will represent a higher fraction of the water pool. Besides, exchange rates R, RM_{0m} and R_{1w} of bound water content are higher than that of free water content. So both RM_{0m} and R_{1w} increase with longer drying time. No significant change in RM_{0w} was observed because of the compromise of the increasing R and decreasing M_{0w}. There is no change in T_{2m} because the short period of air-drying does not affect the macromolecular proton pool much. Further air-drying studies would be interesting to investigate the changes of free water, bound water and macromolecular proton contents when combined with UTE-MT modeling and UTE bi-component analysis (38).

Furthermore, the five MT modeling parameters including f, T_{2m}, R_{1w}, RM_{0m}, and RM_{0w} can be potentially useful biomarkers, especially considering that those biomarkers are insensitive to the magic angle effect (17). Conventional T_2 and T_{1rho} may increase by several fold when the collagen fibers are reoriented from 0° to 55° (the magic angle) relative to the B_0 field (39), while the MT modeling parameters are relatively constant with less than 10% increase near the magic angle (17). The UTE-MT modeling parameters may be useful in the diagnosis and treatment monitoring of osteoporosis, where the macromolecular proton fraction is expected to inversely correlate with cortical porosity. Other MT modeling parameters such as relaxation times and exchange rates may also be correlated with bone properties. Further validation studies on cortical bone samples to correlate UTE MT modeling parameters with micro-CT measurements (cortical porosity, bone mineral content and bone mineral density), and biomechanics including elastic (modulus, yield stress and strain) and failure (ultimate stress, failure strain and energy) properties are still under investigation. The fitted parameter T_{2w} is known to be less accurate, as has been discussed in greater detail in Ref. 40. Lack of consideration of the excitation pulse for this MT model and low duty-cycle of the UTE-MT sequence due to SAR limitation can both lead to inaccurate T_{2w} estimation. For 2D UTE-MT modeling of cortical bone, T_{2w} may be subject to increased error due to the simplification of both bound water and free water into a single water pool. Another way is to measure T_{2w} with fast multi-echo UTE sequences. The curves did not fit the experimental data perfectly, which is probably due to the two-pool approximation. In fact, there are many proton pools in bone tissues including a free water pool, a bound water pool, and a macromolecular pool. Therefore, a two-pool model may not be accurate but just a reasonable approximation where bound water and free water are simplified as one water pool. In addition, there were also biases between the fitting curves and the experimental data for 2D UTE-MT modeling. However, these biases were also present in the Ramani model, which was used to evaluate the cerebral cortex and a multiple sclerosis (MS) lesion (see Fig. 2 in Ref. 15). Though a slight fitting bias exists, their results show that the MT modeling parameters can be good biomarkers to distinguish between normal white matter and MS lesions. We hope the 2D UTE-MT modeling parameters can

similarly provide clinically useful biomarkers of cortical bone properties such as cortical porosity and biomechanical properties. Clearly a lot more research remains to be performed.

Fat has a much higher signal intensity than cortical bone and will also lead to off-resonance and Gibbs ringing artifacts. Therefore, the MT modeling parameters may be affected by fat. Recently, Smith et al. reported that with increased fat fraction, both macromolecular fractions and exchange rates are decreased but T_2 relaxations are increased by numerical simulation (41). To reduce the fat contamination induced errors, they incorporate Dixon multi-echo fat-water separation for fat-free MT modeling. Incorporating fat-water separation methods into UTE-MT modeling can potentially resolve this issue, and will be investigated in future studies.

Simulations have been performed to investigate the effects of B_1 inhomogeneity on MT modeling. From our simulations, if B_1 changes by 5%, the T_1 value measured with the variable TR method will change by 9.3% and MT parameters including f, RM_{0m}, RM_{0w} and R_{1w} will change by 2.3%, 8.9%, 12.9% and 8.7% respectively. There is almost no change for T_{2m}. Therefore, B_1 variation can lead to increased errors in MT quantification, especially for RM_{0m}, RM_{0w} and R_{1w}. On the other hand, a smaller degree of error is observed for f and T_{2m} due to B_1 inhomogeneity. To fully address the errors induced by B_1 variation, correction techniques are needed for accurate MT quantification with a measured B_1 map (42).

There are several limitations to this study. First, we had a small sample size for both ex vivo and in vivo groups. Second, imaging time was clinically prohibitive and longer compared to other bone water quantification methods, including semi-quantitative UTE-MT MTR measurements (12, 14, 37). Some potential strategies to reduce scan time for clinical use include employing fewer datasets, selecting MT powers and frequency offsets using Cramer-Rao lower bounds theory (43), and compressed sensing reconstruction (44). Third, consideration must be given to the level of RF power deposition generated by acquiring MT data at different MT pulse powers and off-resonance frequencies. This may ultimately impact the dynamic range of quantitative UTE-MT acquisitions. Lastly, most of the previously reported quantitative MT models assume only two pools of protons (water and macromolecular protons) (13, 15, 16), theoretically however, a three-pool model (free water, bound water, and macromolecular protons) would be more accurate than the two-pool model for evaluating biological tissues (45).

In conclusion, we provided preliminary data for UTE-MT modeling in ex vivo bovine and healthy adult cortical bone. This technique allows for a more comprehensive assessment of the MT process than previously reported by MTR measurement alone and lays the ground work for future studies into disease-based changes in MT parameters. We believe that UTE-MT modeling has the potential to provide a complementary quantitative approach to the diagnosis and treatment of conditions associated with impaired bone quality.

Acknowledgments

References

1. Nazrun AS, Tzar MN, Mokhtar SA, Mohamed IN. A systematic review of the outcomes of osteoporotic fracture patients after hospital discharge: morbidity, subsequent fractures, and mortality. Ther Clin Risk Manag. 2014; 10:937–48. [PubMed: 25429224]

2. Johnell O, Kanis J. Epidemiology of osteoporotic fractures. Osteoporosis international : a journal established as result of cooperation between the European Foundation for Osteoporosis and the National Osteoporosis Foundation of the USA. 2005; 16(Suppl 2):S3–7.

3. Cummings SR, Karpf DB, Harris F, Genant HK, Ensrud K, LaCroix AZ, et al. Improvement in spine bone density and reduction in risk of vertebral fractures during treatment with antiresorptive drugs. Am J Med. 2002; 112(4):281–9. [PubMed: 11893367]

4. Schuit SC, van der Klift M, Weel AE, de Laet CE, Burger H, Seeman E, et al. Fracture incidence and association with bone mineral density in elderly men and women: the Rotterdam Study. Bone. 2004; 34(1):195–202. [PubMed: 14751578]

5. Sornay-Rendu E, Munoz F, Garnero P, Duboeuf F, Delmas PD. Identification of osteopenic women at high risk of fracture: the OFELY study. J Bone Miner Res. 2005; 20(10):1813–9. [PubMed: 16160738]

6. Majumdar S, Genant HK, Grampp S, Newitt DC, Truong VH, Lin JC, et al. Correlation of trabecular bone structure with age, bone mineral density, and osteoporotic status: in vivo studies in the distal radius using high resolution magnetic resonance imaging. J Bone Miner Res. 1997; 12(1): 111–8. [PubMed: 9240733]

7. Reichert IL, Robson MD, Gatehouse PD, He T, Chappell KE, Holmes J, et al. Magnetic resonance imaging of cortical bone with ultrashort TE pulse sequences. Magn Reson Imaging. 2005; 23(5): 611–8. [PubMed: 16051035]

8. Bae WC, Chen PC, Chung CB, Masuda K, D'Lima D, Du J. Quantitative ultrashort echo time (UTE) MRI of human cortical bone: correlation with porosity and biomechanical properties. J Bone Miner Res. 2012; 27(4):848–57. [PubMed: 22190232]

9. Du J, Carl M, Bydder M, Takahashi A, Chung CB, Bydder GM. Qualitative and quantitative ultrashort echo time (UTE) imaging of cortical bone. J Magn Reson. 2010; 207(2):304–11. [PubMed: 20980179]

10. Techawiboonwong A, Song HK, Leonard MB, Wehrli FW. Cortical bone water: in vivo quantification with ultrashort echo-time MR imaging. Radiology. 2008; 248(3):824–33. [PubMed: 18632530]

11. Henkelman RM, Stanisz GJ, Graham SJ. Magnetization transfer in MRI: a review. NMR Biomed. 2001; 14(2):57–64. [PubMed: 11320533]

12. Syha R, Martirosian P, Ketelsen D, Grosse U, Claussen CD, Schick F, et al. Magnetization transfer in human Achilles tendon assessed by a 3D ultrashort echo time sequence: quantitative examinations in healthy volunteers at 3T. RoFo : Fortschritte auf dem Gebiete der Rontgenstrahlen und der Nuklearmedizin. 2011; 183(11):1043–50. [PubMed: 21986866]

13. Hodgson RJ, Evans R, Wright P, Grainger AJ, O'Connor PJ, Helliwell P, et al. Quantitative magnetization transfer ultrashort echo time imaging of the Achilles tendon. Magn Reson Med. 2011; 65(5):1372–6. [PubMed: 21500263]

14. Chang EY, Bae WC, Shao H, Biswas R, Li S, Chen J, et al. Ultrashort echo time magnetization transfer (UTE-MT) imaging of cortical bone. NMR Biomed. 2015; 28(7):873–80. [PubMed: 25981914]

15. Ramani A, Dalton C, Miller DH, Tofts PS, Barker GJ. Precise estimate of fundamental in-vivo MT parameters in human brain in clinically feasible times. Magn Reson Imaging. 2002; 20(10):721–31. [PubMed: 12591568]

16. Henkelman RM, Huang X, Xiang QS, Stanisz GJ, Swanson SD, Bronskill MJ. Quantitative interpretation of magnetization transfer. Magn Reson Med. 1993; 29(6):759–66. [PubMed: 8350718]

17. Ma YJ, Shao H, Du J, Chang EY. Ultrashort echo time magnetization transfer (UTE-MT) imaging and modeling: magic angle independent biomarkers of tissue properties. NMR Biomed. 2016; 29(11):1546–52. [PubMed: 27599046]

18. Du J, Bydder GM. Qualitative and quantitative ultrashort-TE MRI of cortical bone. 2013; 26:489–508.

19. Chen J, Chang EY, Carl M, Ma Y, Shao H, Chen B, Wu Z, Du J. Measurement of bound and pore water T1 relaxation times in cortical bone using three - dimensional ultrashort echo time cones sequences. Magn Reson Med. 2016; doi: 10.1002/mrm.26292

20. Horch RA, Nyman JS, Gochberg DF, Dortch RD, Does MD. Characterization of 1H NMR signal in human cortical bone for magnetic resonance imaging. Magn Reson Med. 2010; 64(3):680–7. [PubMed: 20806375]

21. Biswas R, Bae W, Diaz E, Masuda K, Chung CB, Bydder GM, et al. Ultrashort echo time (UTE) imaging with bi-component analysis: bound and free water evaluation of bovine cortical bone subject to sequential drying. Bone. 2012; 50(3):749–55. [PubMed: 22178540]

22. Nyman JS, Ni Q, Nicolella DP, Wang X. Measurements of mobile and bound water by nuclear magnetic resonance correlate with mechanical properties of bone. Bone. 2008; 42(1):193–9. [PubMed: 17964874]

23. Ong HH, Wright AC, Wehrli FW. Deuterium nuclear magnetic resonance unambiguously quantifies pore and collagen-bound water in cortical bone. J Bone Miner Res. 2012; 27(12):2573–81. [PubMed: 22807107]

24. McCalden RW, McGeough JA, Barker MB, Court-Brown CM. Age-related changes in the tensile properties of cortical bone. The relative importance of changes in porosity, mineralization, and microstructure. J Bone Joint Surg Am. 1993; 75(8):1193–205. [PubMed: 8354678]

25. Ahmed LA, Shigdel R, Joakimsen RM, Eldevik OP, Eriksen EF, Ghasem-Zadeh A, et al. Measurement of cortical porosity of the proximal femur improves identification of women with nonvertebral fragility fractures. Osteoporosis international : a journal established as result of cooperation between the European Foundation for Osteoporosis and the National Osteoporosis Foundation of the USA. 2015; 26(8):2137–46.

26. Schaffler MB, Burr DB. Stiffness of compact bone: effects of porosity and density. J Biomech. 1988; 21(1):13–6. [PubMed: 3339022]

27. Nyman JS, Roy A, Tyler JH, Acuna RL, Gayle HJ, Wang X. Age-related factors affecting the postyield energy dissipation of human cortical bone. J Orthop Res. 2007; 25(5):646–55. [PubMed: 17266142]

28. Basillais A, Bensamoun S, Chappard C, Brunet-Imbault B, Lemineur G, Ilharreborde B, et al. Three-dimensional characterization of cortical bone microstructure by microcomputed tomography: validation with ultrasonic and microscopic measurements. J Orthop Sci. 2007; 12(2):141–8. [PubMed: 17393269]

29. Rajapakse CS, Bashoor-Zadeh M, Li C, Sun W, Wright AC, Wehrli FW. Volumetric Cortical Bone Porosity Assessment with MR Imaging: Validation and Clinical Feasibility. Radiology. 2015; 276(2):526–35. [PubMed: 26203710]

30. Manhard MK, Horch RA, Gochberg DF, Nyman JS, Does MD. In Vivo Quantitative MR Imaging of Bound and Pore Water in Cortical Bone. Radiology. 2015; 277(3):927.

31. Springer F, Martirosian P, Machann J, Schwenzer NF, Claussen CD, Schick F. Magnetization transfer contrast imaging in bovine and human cortical bone applying an ultrashort echo time sequence at 3 Tesla. Magn Reson Med. 2009; 61(5):1040–8. [PubMed: 19267348]

32. Ridha BH, Tozer DJ, Symms MR, Stockton KC, Lewis EB, Siddique MM, et al. Quantitative magnetization transfer imaging in Alzheimer disease. Radiology. 2007; 244(3):832–7. [PubMed: 17709831]

33. Tozer D, Ramani A, Barker GJ, Davies GR, Miller DH, Tofts PS. Quantitative magnetization transfer mapping of bound protons in multiple sclerosis. Magn Reson Med. 2003; 50(1):83–91. [PubMed: 12815682]

34. Sinclair CD, Samson RS, Thomas DL, Weiskopf N, Lutti A, Thornton JS, et al. Quantitative magnetization transfer in in vivo healthy human skeletal muscle at 3 T. Magn Reson Med. 2010; 64(6):1739–48. [PubMed: 20665899]

35. Li C, Seifert AC, Rad HS, Bhagat Y, Rajapakse CS, Sun W, et al. Cortical Bone Water Concentration: Dependence of MR Imaging Measures on Age and Pore Volume Fraction. Radiology. 2014:132585.

36. Rad HS, Lam SC, Magland JF, Ong H, Li C, Song HK, et al. Quantifying cortical bone water in vivo by three-dimensional ultra-short echo-time MRI. NMR Biomed. 2011; 24(7):855–64. [PubMed: 21274960]

37. Unnanuntana A, Gladnick BP, Donnelly E, Lane JM. The assessment of fracture risk. J Bone Joint Surg Am. 2010; 92(3):743–53. [PubMed: 20194335]

38. Biswas R, Bae W, Diaz E, Masuda K, Chung CB, Bydder GM, Du J. Ultrashort echo time (UTE) imaging with bi-component analysis: Bound and free water evaluation of bovine cortical bone subject to sequential drying. Bone. 2012; 50:749–755. [PubMed: 22178540]

39. Shao H, Pauli C, Li S, Ma Y, Tadros AS, Chang EY, Du J. Magic angle effect plays a significant role in T1rho relaxation in articular cartilage. Osteoarthritis Cartilage. 2017; doi: 10.1016/j.joca.2017.01.013

40. Cercignani M, Barker GJ. A comparison between equations describing in vivo MT: the effects of noise and sequence parameters. J Magn Reson. 2008; 191:171–183. [PubMed: 18191599]

41. Smith AK, Dortch RD, Dethrage LM, Lyttle BD, Kang H, Welch EB, Smith SA. Incorporating novel quantitative magnetization transfer of the human optic nerve in vivo. Magnetic resonance in medicine. 2017 Feb 1; 77(2):707–16. [PubMed: 27037720]

42. Yarnykh VL. Optimal radiofrequency and gradient spoiling for improved accuracy of T1 and B1 measurements using fast steadystate techniques. Magn Reson Med. 2010; 63:1610–1626. [PubMed: 20512865]

43. Cercignani M, Alexander DC. Optimal acquisition schemes for in vivo quantitative magnetization transfer MRI. Magn Reson Med. 2006; 56(4):803–10. [PubMed: 16902982]

44. Lustig M, Donoho D, Pauly JM. Sparse MRI: The application of compressed sensing for rapid MR imaging. Magn Reson Med. 2007; 58(6):1182–95. [PubMed: 17969013]

45. Ceckler T, Maneval J, Melkowits B. Modeling magnetization transfer using a three-pool model and physically meaningful constraints on the fitting parameters. J Magn Reson. 2001; 151(1):9–27. [PubMed: 11444932]
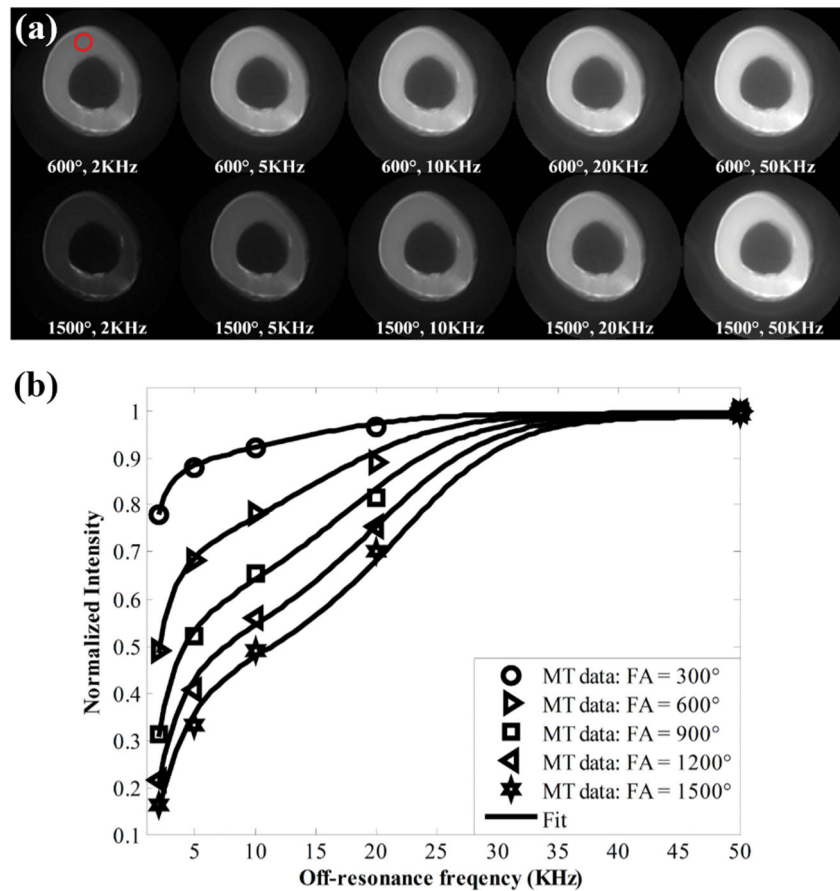
Figure 1.
(**a**) Representative MT images from an ex vivo bovine cortical bone specimen obtained with MT flip angles of 600° and 900° at increasing off-resonance frequencies of 2, 5,10, 20, and 50 kHz. (**b**) Fitting curves for cortical bone signal intensity versus off-resonance frequency for multiple MT flip angles are shown. Increased cortical bone signal intensity is observed at low MT flip angles and high off-resonance frequencies. Red circle in top left MT image (600°, 2 kHz) (**a**) shows region of interest used for signal intensity measurement.
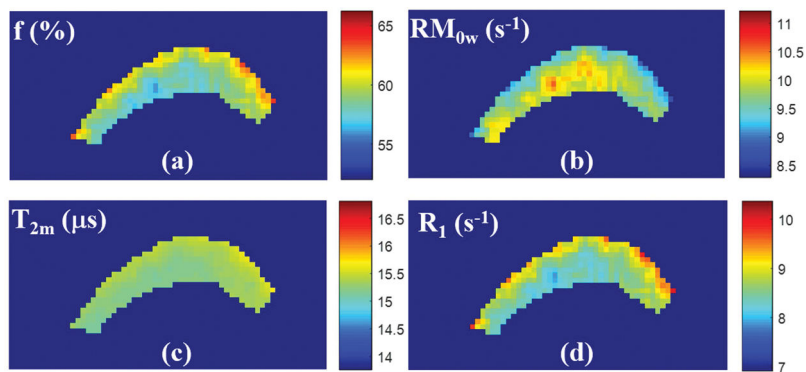
Figure 2.
Color mapping of MT modeling parameters from an ex vivo bovine cortical bone specimen, including macromolecular fraction (f) (**a**), proton exchange rate from the macromolecular to water pools (RM_{0w}) (**b**), T_2 relaxation time of the macromolecular pool (T_{2m}) (**c**), and spin-lattice relaxation rate of the water pool (R_{1w}) (**d**). Color maps demonstrate good homogeneity of MT modeling values within cortical bone. Color bar indicates the gradation of MT modeling measures.
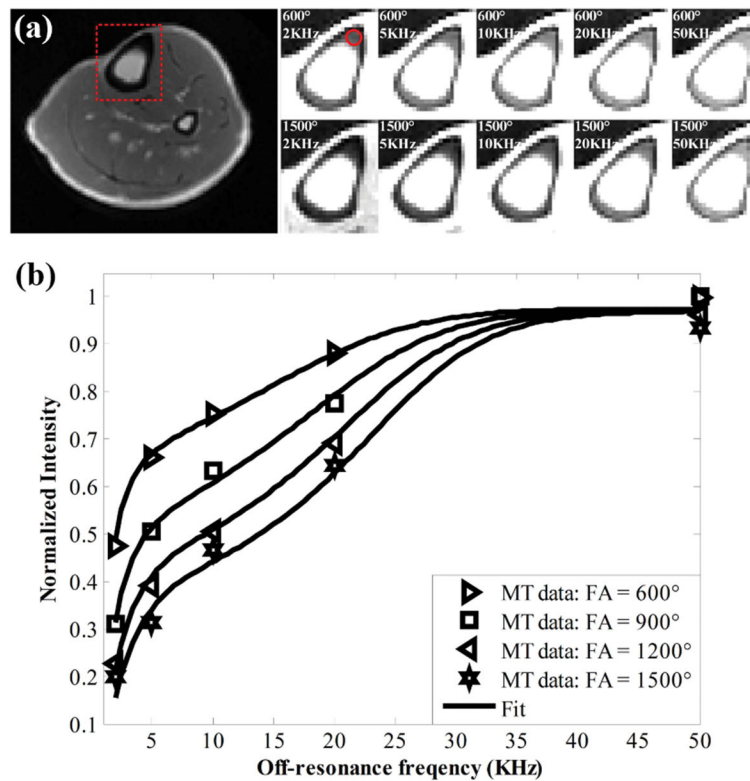
Figure 3.
(**a**) Representative MT images from in vivo human tibial cortical bone obtained with MT flip angles of 600° and 900° at increasing off-resonance frequencies of 2, 5, 10, 20, and 50 kHz. (**b**) Fitting curves for cortical bone signal intensity versus off-resonance frequency for multiple MT flip angles are shown. Similar to bovine cortical bone, increased signal intensity is evident at low MT flip angles and high off-resonance frequencies. Red dashed box in far-left image (**a**) shows field of view selection for MT analysis. Red circle in top left MT image (600°, 2 kHz) (**a**) shows region of interest used for signal intensity measurement.
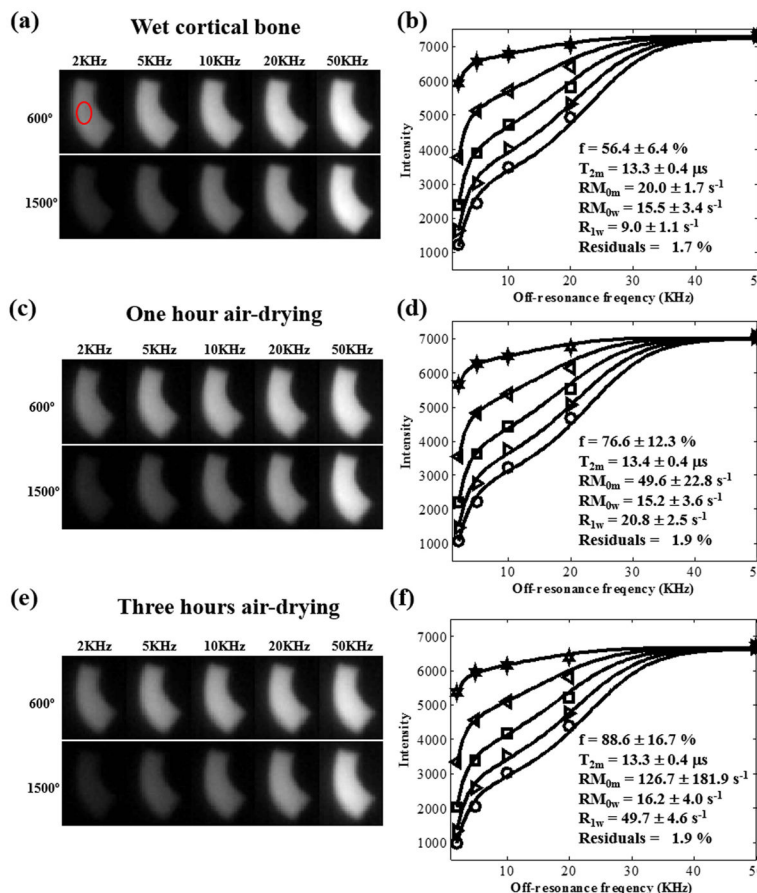
Figure 4.
(**a**), (**c**) and (**e**) are representative MT images from the sequential air-drying bovine cortical bone study (i.e. wet bone, one hour of drying and three hours of drying) obtained with MT flip angles of 600° and 900° at increasing off-resonance frequencies of 2, 5,10, 20, and 50 kHz. (**b**), (**d**) and (**f**) are corresponding fitting curves for cortical bone signal intensity versus off-resonance frequency for multiple MT flip angles are shown. Red circle in top left MT image (600°, 2 kHz) (**a**) shows region of interest used for signal intensity measurement. The sequential MT modeling results are also shown in (**b**), (**d**) and (**f**).

Table 1

Quantitative MT modeling measurements[*] for ex vivo bovine cortical bone (N = 5).

	f (%)	T_{2m} (µs)	R_{1w} (s^{-1})	RM_{0m} (s^{-1})	RM_{0w} (s^{-1})	Residuals (%)
1	57.4	14.5	8.9	15.5	11.5	1.7
2	59.6	14.7	9.5	16.2	11	1.7
3	71.4	14.8	13.9	24.3	9.7	1.9
4	59.6	14.7	9.4	17.2	11.7	1.8
5	51.5	14.1	7.6	16.1	15.2	1.9

[*]
f = macromolecular fraction; T_{2m} = T_2 relaxation time of macromolecular pool; R_{1w} = spin-lattice relaxation rate of water pool; RM_{0m} = proton exchange rate from water to macromolecular pool; RM_{0w} = proton exchange rate from macromolecular to water pool, Residuals = Residual of fitting.

Table 2

Quantitative MT modeling measurements [*] for in vivo human tibial cortical bone (N = 5).

	f (%)	T_{2m} (µs)	R_{1w} (s^{-1})	RM_{0m} (s^{-1})	RM_{0w} (s^{-1})	Residuals (%)
1	61.3	15.5	10.6	13.6	8.6	2.9
2	54.2	16.0	9.4	8.6	7.3	2.3
3	51.1	15.6	8.1	10.1	9.7	2.8
4	48.8	15.5	7.8	8.8	9.3	2.5
5	56.9	14.4	8.7	16.6	12.5	2.9

[*]
f = macromolecular fraction; T_{2m} = T_2 relaxation time of macromolecular pool; R_{1w} = spin-lattice relaxation rate of water pool; RM_{0m} = proton exchange rate from water to macromolecular pool; RM_{0w} = proton exchange rate from macromolecular to water pool, Residuals = Residual of fitting.